Title: Increased neuronal expression of the early endosomal adaptor APPL1 leads to endosomal and synaptic dysfunction with cholinergic neurodegeneration.

Abbreviated title: APPL1 transgenic mice reproduce AD endosomal pathology.

Ying Jiang[1,2]; Kuldeep Sachdeva[1,2]; Chris N. Goulbourne[1]; Martin J. Berg[1]; James Peddy[1]; Philip H. Stavrides[1]; Anna Pensalfini[1]; Monika Pawlik[1]; Lauren Whyte[1]; Basavaraj S. Balapal[1,2]; Subbanna Shivakumar[1], Cynthia Bleiwas[1]; John F. Smiley[2,3]; Paul M. Mathews[1,2,4] and Ralph A. Nixon[1,2,4,5*]

[1]Center for Dementia Research, Nathan S. Kline Institute for Psychiatric Research, Orangeburg, NY 10962, USA

[2]Department of Psychiatry, New York University Grossman School of Medicine, New York, NY 10016, USA

[3]Emotion Brain Institute, Nathan S. Kline Institute for Psychiatric Research, Orangeburg, NY 10962, USA

[4]Department of Cell Biology, [5]Neuroscience Institute, New York University Grossman School of Medicine, New York, NY 10016, USA

*Corresponding Author: Ralph A Nixon, MD, PhD, Nathan S. Kline Institute for Psychiatric Research, 140 Old Orangeburg Road, Orangeburg, NY, 10962, USA. P: 845-398-5423; F: 845-398-5422, nixon@nki.rfmh.org

Acknowledgments

The study was supported by NIH grants P01AG017617 and R01AG062376 grants to R.A.N.

B.S.B. and S.S. are supported by NIH grant RO1AA29686.

Author contributions

R.A.N. and Y.J. designed the research; Y.J., K.S., M.J.B., S.S., B.S.B., C.B., J.F.S., C.N.G., M.P., P.H.S., J.P., A.P., and L.W. conducted the research; Y.J. wrote the first draft; Y.J., P.M.M., and R.A.N. edited the paper.

Declaration of interest

The authors declare no competing interests.

Keywords

APPL1, AD, rab5, APP-βCTF, synaptosome, endosome, ChAT+ neuron, LTD, LTP.

Abbreviations

AD=Alzheimer's disease; APPL1=adaptor protein containing pleckstrin homology domain, phosphotyrosine binding domain (PTB), and leucine zipper motif; ChAT=choline acetyltransferase; MSN=medial septal nucleus; LTD=long-term depression; LTP=long-term potentiation; PHF1=phosphorylated tau; SVE=synaptic vesicle endocytosis.

Abstract

Dysfunction of the endolysosomal system within neurons is a prominent feature of Alzheimer's disease (AD) pathology. Multiple AD-risk factors are known to cause hyper-activity of the early-endosome small GTPase rab5, resulting in neuronal endosomal pathway disruption. APPL1, an important rab5 effector protein, is an interface between endosomal and neuronal function through a rab5-activating interaction with the BACE1-generated C-terminal fragment (βCTF or C99) of the amyloid precursor protein (APP), a pathogenic APP fragment generated within endolysosomal compartments. To better understand the role of APPL1 in the AD endosomal phenotype, we generated a transgenic mouse model over-expressing human APPL1 within neurons (Thy1-APPL1 mice). Consistent with the important endosomal regulatory role of APPL1, Thy1-APPL1 mice have enlarged neuronal early endosomes and increased synaptic endocytosis due to increased rab5 activation. We additionally demonstrate pathological consequences of APPL1 overexpression, including functional changes in hippocampal long-term potentiation (LTP) and long-term depression (LTD), as well as degeneration of the large projection cholinergic neurons of the basal forebrain and impairment of hippocampal-dependent memory. Our findings show that increased neuronal APPL1 levels lead to a cascade of pathological effects within neurons, including early endosomal alterations, synaptic dysfunction, and neurodegeneration. Multiple risk factors and molecular regulators, including APPL1 activity, are known to contribute to the endosomal dysregulation seen in the early stages of AD, and these findings further highlight the shared pathobiology and consequences to a neuron of early endosomal pathway disruption.

Significance Statement

Dysfunction in the endolysosomal system within neurons is a key feature of Alzheimer's disease (AD). Multiple AD risk factors lead to hyperactivity of the early-endosome GTPase rab5, disrupting neuronal pathways including the cholinergic circuits involved early in memory

decline. APPL1, a crucial rab5 effector, connects endosomal and neuronal functions through its interaction with a specific amyloid precursor protein (APP) fragment generated within endosomes. To understand APPL1's role, a transgenic mouse model over-expressing human APPL1 in neurons (Thy1-APPL1 mice) was developed. These mice show enlarged early endosomes and increased synaptic endocytosis due to rab5 activation, resulting in impaired hippocampal long-term potentiation and depression, the degeneration of basal forebrain cholinergic neurons, and memory deficits, highlighting a pathological cascade mediated through APPL1 at the early endosome.

1. Introduction

Endosomal pathway dysfunction within neurons is one of the earliest pathologies of AD, with evidence arguing that endosomal changes occur years, if not decades, prior to the hallmark pathologies of β-amyloid and PHF tau accumulation (Cataldo et al., 2000; Colacurcio et al., 2018; Pensalfini et al., 2020; Fahimi et al., 2021). For example, expression of the apolipoprotein E ε4 allele, the most significant genetic risk factor for AD, drives neuronal endosomal alterations in humans (Cataldo et al., 2000) as well as in mouse models, where these changes are independent of any β-amyloid or tau pathology (Nuriel et al., 2017; Peng et al., 2024). Trisomy 21 (Down syndrome (DS)), which inevitably leads to AD in mid-life, leads to life-long early endosome disruption through a mechanism dependent upon the intracellular accumulation of the BACE1 β-cleaved C-terminal fragment of the amyloid precursor protein (APP-βCTF, C99) (Jiang et al., 2016; Kim et al., 2016; Nixon et al., 2017; Colacurcio et al., 2018; Lauritzen et al., 2019). Additionally, neuronal endosomal pathology has been shown in mouse models in which APP-βCTF levels are increased following APP overexpression (Choi et al., 2013; Lauritzen et al., 2016; Bourgeois et al., 2018), and APP-βCTF levels are increased in human AD brain tissue compared to control (Pera et al., 2013; Kim et al., 2016). These findings from diverse *in vitro* and *in vivo* models and human tissue provide compelling evidence that an increase in APP-βCTFs within a neuron can directly drive early endosomal dysfunction, altering their morphology, disrupting endolysosomal trafficking, and leading to neuron loss (Jiang et al., 2010; Jiang et al., 2016; Lauritzen et al., 2016; Nixon et al., 2017; Bourgeois et al., 2018; Colacurcio et al., 2018).

The neuronal endosome enlargement and proliferation seen in late-onset AD cases involves the recruitment and activation of the master-signaling GTPase rab5 on early endosomal membranes. Rab5, in its GTP-bound state, interacts with the early endosomal membrane as well as an extensive cohort of adaptor and regulatory molecules that, in concert, define an early

endosome and its complex sorting and trafficking functions (Langemeyer et al., 2018). Hyper-function of rab5, achieved by moderate overexpression in neurons of rab5, is sufficient to recapitulate AD-related early endosome changes as well as their neurodegenerative consequences, prominently seen in cholinergic neurons in the basal forebrain (Kim et al., 2016; Pensalfini et al., 2020). Kim et al. (Kim et al., 2016) demonstrated that the molecular cascade linking rab5 overactivation and APP-βCTF levels includes the endosome adaptor protein APPL1 (Adaptor protein containing a Pleckstrin homology domain, a Phosphotyrosine binding (PTB), and a Leucine zipper motif 1) (Miaczynska et al., 2004; Zhu et al., 2007). APPL1 interacts with rab5 at the early endosomal membrane and is an important modulator of endocytic trafficking known to interface with an array of structural and signaling proteins (Diggins and Webb, 2017). For example, APPL1 modulates Akt signaling processes (Majumdar et al., 2011; Bohdanowicz et al., 2012; Wang et al., 2016; Goto-Silva et al., 2019) and mediates nerve growth factor signaling through TrkA (Lin et al., 2006). Indeed, APPL1's PTB binding domain allows it to couple membrane trafficking with diverse signaling functions (Diggins and Webb, 2017), bridging a diversity of functions at the early endosome. APPL1 has been shown to be important to hippocampal synaptic plasticity (Formolo et al., 2022) by regulating trafficking and sorting at the early endosome. Following rab5 GTP hydrolysis, APPL1 is released from the early endosomal membrane and has been shown to be capable of being translocated to the nucleus to subsequently regulate gene expression (Zoncu et al., 2009; Rashid et al., 2009), placing APPL1 function within a complex web of endosome functions and endocytic responses.

The APP-βCTF directly binds and recruits to endosomal APPL1, which in the homodimer conformation stabilizes the GTP-bound state of rab5, the molecular switch that increases rab5 function and, in states of rab5 over-activation, leads to early endosome disruption (Kim et al., 2016). This rab5/APPL1/APP-βCTF interaction was shown to accelerate endocytosis, driving

endosome enlargement and impairing the axonal transport of endosomes in cultured neuronal cells when APP-βCTF levels were elevated following APP overexpression (Kim et al., 2016). APPL1 levels also appear to be increased in AD. Proteomics analyses from the Religious Orders Study revealed a two-times increase of APPL1 protein in the brains of AD individuals compared to age-matched controls (Johnson et al., 2022), and APPL1 protein has been shown to accumulate in CA1 neurons in AD patients (Ogawa et al., 2013).

To better examine the interface between APPL1 function and the diverse endosomal and neurodegenerative consequences attributed to early endosome dysfunction in AD pathobiology, we generated a novel transgenic mouse model that overexpresses APPL1 in neurons (Thy1-APPL1 mice). With moderate APPL1 expression (2-times), this Thy1-APPL1 model exhibited enlarged rab5-positive endosomes in cortical neurons, coupled with increased rab5 activation compared to wild-type littermates. Thy1-APPL1 mice had increased levels of rab5 protein in isolated hippocampal synaptosomes, a finding consistent with a higher rate of endocytosis in synaptosomes. Hippocampal synaptic function assessed by long-term potentiation (LTP) and long-term depression (LDP) was found to be altered in Thy1-APPL1 mice compared to that of wild-type mice. The number of choline acetyltransferase (ChAT)-positive neurons in medial septal nucleus (MSN) was reduced in Thy1-APPL1 mice and hippocampal-dependent memory, as measured by the novel object recognition test, was impaired. These results support the idea that APPL1 recruitment and over activation is sufficient to link APP-βCTF levels and rab5 activation (Kim et al., 2016) to the endosomal, functional, and neurodegenerative changes seen in a diverse range of AD endosomal-pathology models (Jiang et al., 2016; Nixon et al., 2017; Jiang et al., 2022; Peng et al., 2024).

2. Methods

2.1. Thy-APPL1 transgene construct, generation of transgenic mice, and genotyping.

Transgenic mice overexpressing human APPL1 (NM_012096) were generated by Ingenious Targeting Laboratory (Ronkonkoma, NY) using the pTSC21 vector consisting of a murine Thy1 expression cassette (Pensalfini et al., 2020) and a Flag-tag for identification. Two founder mice (M1 and F2) were obtained on a mixed background of 129SvEC and C57BL/6, which were then crossed with C57BL/6 mice (JAX stock number 000664, The Jackson Laboratory, Bar Harbor, ME) for over 10 generations to establish the line used in this study; offspring from F2 founder mice were studied. Thy1-APPL1 mice genotyping was accomplished by PCR using the following primer pair: forward-5' ATGAAGTCACCCAGCAGGGAG and reverse 5' AGGTCAGGTGTGTTGCTGCAC. Each reaction consisted of H_2O (23 µl), 2X GO Taq master mix (M7122, Promega), primer pair (0.5 µl each), and tail DNA (1 µl of a 0.05-0.1 mg/ml solution). PCR conditions were as follows: 94°C for 3 minutes, followed by 30 cycles of 94°C for 30 seconds, 58°C for 30 seconds, and 72°C for 30 seconds, with a final extension step at 72°C for 5 minutes. The reaction mixes were then loaded onto agarose gels, and positive Thy1-APPL1 mouse samples produced a band at or above 500 bp. Thy-APPL1 bred normally with the expected Mendelian ratio of offsprings, with normal body weight and lifespan. Throughout, non-Tg littermates were used as control, wild-type mice.

Mouse experimentation and animal care was approved by the Institutional Animal Care and Use Committee (IACUC) of the Nathan S. Kline Institute. The approval is renewed every three years, and the current protocol number is AP2021-685. Mice were housed in the NKI Animal facility and kept under a 12-hour day and night cycle, at temperatures of approximately 70°F (±2°C) and humidity between 40% and 60%. Both male and female mice were used.

2.2. Immunocytochemistry and Western blot analysis.

Thy-APPL1 mice and their age-matched littermates (non-transgenic: non-Tg) were anesthetized with a combination of ketamine (100 mg/kg BW) and xylazine (10 mg/kg BW) and transcardially perfused with phosphate-buffered saline solution as described earlier (Pensalfini et al., 2020; Jiang et al., 2022). One hemibrain was frozen and stored at -80^{0}C for biochemistry (see below) with the remaining hemibrain drop-fixed in 4% paraformaldehyde in 0.1M sodium cacodylate buffer, pH 7.4 (Electron Microscopy Sciences EMS) for immunolabeling. After fixation, 40-µm thick vibratome brain tissue sections were washed three times with antibody dilution buffer containing bovine serum albumin (BSA; 1%; Sigma), saponin (0.05%; Sigma), and normal horse serum (NHS; 1%; Thermo Fisher) in Tris-buffered saline (TBS, pH 7.4), then blocked with 20% NHS in TBS for one hour at room temperature before incubation with commercial antibodies against APPL1 (Novus Cat#NBP2-46536; RRID:AB_3083472; 1:500), rab5 (Abcam Cat# ab218624, RRID:AB_28927171:500), rab5-GTP (active rab5: NewEast Biosciences Cat# 26911, RRID:AB_2617182; 1:50), ChAT (Millipore Cat# AB144P, RRID:AB_20797511:250), APPL1 (Proteintech Cat# 12639-1-AP, RRID:AB_2289669; 1:500), and the Flag-tag (Thermo Fisher Scientific Cat# MA1-91878-D488, RRID:AB_2537621; 1:500), either alone or in combination and visualized with either biotinylated secondary antibodies (Vector Laboratories; Cat# BA-9200, BA-1000 and BA-6000; 1:500) or fluorescence-conjugated secondary antibodies (Thermo Fisher; Cat# A10037, A21206 and A21099;1:500), as described in our previous studies (Pensalfini et al., 2020; Jiang et al., 2022). Confocal images were collected using a Zeiss LSM880 laser confocal microscope and Zen 2.1-Sp3 software. Rab5 and rab5-GTP positive puncta, including intensity, number, average size, and total area per cell, was determined by Fiji/ImageJ 2.3.0 (https://imagej.net/Fiji). Three or more mice per genotype were analyzed, and 20-30 neurons from each mouse were quantified (Pensalfini et al., 2020; Jiang et al., 2022). For protein

analyses, mouse hemi-brains were homogenized in 1:10 (brain weight: buffer) pH 7.4 buffer containing 250 mM sucrose, 20mM Tris-HCl, 1mM EDTA, 1mM EGTA, protease/phosphatase inhibitors (Pensalfini et al., 2020; Jiang et al., 2022), and western blot analyses as described previously were performed with antibodies against APP (C1/6.1; 1:1000) (Jiang et al., 2010), APP-βCTF (M3.2; 1:1000 (Morales-Corraliza et al., 2009), APPL1 (Proteintech; 1:1000), rab5 (Abcam; 1:2000), synaptophysin (Sigma-Aldrich Cat# S5768, RRID:AB_477523; 1:2000), phosphorylated tau (PHF1; 1:1000, kind gift of P. Davies (Pensalfini et al., 2020) and total tau protein (Agilent Cat# A0024, RRID:AB_10013724; 1:5000). All the secondary antibodies for western blot analyses were used according to the manufacturer's recommendations (Jackson ImmunoResearch Laboratories, PA). As an internal loading control, total protein on each blot was determined following staining by Revert™ 700 Total protein Stain (Licor; Cat# 926-11021), and a digital gel imager (Syn-gene G:Box XX9) was used to capture both the total protein stain and the ECL images from each blot. Band intensities on each blot were quantified with a combination of Fiji/ImageJ 2.3.0. and Multi Gauge (Fujifilm; V3.0).

2.3. ELISA of Aβ40 and Aβ42 of DEA extracts from brain tissue of Thy1-APPL1 and non-Tg mice.

Aβ40 and Aβ42 levels were determined by sandwich ELISA according to previously published protocols (Schmidt et al., 2012; Jiang et al., 2016). Briefly, brain homogenates were extracted with 0.4% diethylamine (Sigma, Cat# D3131) /100 mM NaCl solution (1:1 of V:V), then processed further with a tissue grinder before centrifugation at 43,000 rpm for one hour at 4ºC in a Beckman Coulter TLA 100.3 rotor. The collected supernatants were mixed with 10% volume of 0.5 M Tris buffer (pH 6.8) and 100 µl of the buffered samples were loaded into ELISA plates ELISA plates coated with specific anti-Aβ40 or Aβ42 antibodies as reported previously (Schmidt et al., 2005; Jiang et al., 2016). Horseradish peroxidase (HRP) conjugated

secondary antibody (M3.2, 1:1000) (Choi et al., 2009; Jiang et al., 2016) was used for both Aβ40 and Aβ42 detections, and a multimode plate reader (SpectraMax M5, Molecular Devices) was used to read the O.D.450nm. The level of Aβ40 or Aβ42 was presented in fmol/g of brain tissue, calculated according to a standard curve using synthetic mouse Aβ40 or Aβ42 peptides (American Peptide Co.) (Choi et al., 2009; Jiang et al., 2016; Pensalfini et al., 2020).

2.4. Stereological counting of medial septal nucleus ChAT-immunoreactive neurons.

For ChAT immunolabeling, every third consecutive vibratome brain tissue section containing medial septal nucleus (MSN) was treated with 3% H_2O_2 before blocking and then incubated with an anti-ChAT antibody (Millipore Sigma; 1:250) as described previously (Jiang et al., 2016; Jiang et al., 2022). Visualization was achieved using diaminobenzidine (DAB; Cat# SK-4100; Vector Laboratories) after incubation with a biotinylated secondary antibody (1:500; Vector Laboratories) and the Vectastain ABC kit (Vector Laboratories Cat# PK6105,). To quantify ChAT-positive neuron in the MSN, the optical fractionator method was used with ImageJ software and a Nikon Eclipse E600 microscope equipped with a 100x oil immersion objective, as previously described (Jiang et al., 2016; Jiang et al., 2022). ChAT-positive neurons were viewed using a grid of optical dissector counting sites, and a z-stack of six images was captured with 1.5-micron spacing. Cell counts were corrected for the z-axis section thickness, which was measured three times per section. The dissector size and density were optimized to maintain a coefficient of error consistently below 0.1.

2.5. Electrophysiology.

Thy1-APPL1 and non-Tg littermate mice (n=5 for each genotype) were used to measure long-term potentiation (LTP) and long-term depression (LTD) in the hippocampal CA1 as detailed in previous studies (Subbanna et al., 2013; Pensalfini et al., 2020). For both LTP and LTD experiments, a 10-minutes baseline was recorded at 1-minute intervals. The intensity of the stimulus was set to evoke a response that is approximately 35% of the maximum evoked

response. LTP was induced using theta-burst stimulation (4 pulses at 100 Hz, with the bursts repeated at 5 Hz, and each tetanus, including three 10-burst trains separated by 15 seconds) and LTD was induced using 1 Hz for 900 seconds. LTP responses were recorded for 2 hours, while LTD responses were recorded for 80 minutes. The results are expressed as both slopes and bar graphs (mean ± SEM) showing individual mouse data versus time points as previously reported (Subbanna et al., 2013; Pensalfini et al., 2020).

2.6. Electron Microscopy and post-embedding immunogold EM.

Electron microscopy and post-embedding immunogold EM were performed on brain sections as previously described (Yang et al., 2009; Pensalfini et al., 2020). Mice were transcardially perfused with a solution of 4% PFA and 2% glutaraldehyde in 0.1 M sodium cacodylate buffer, pH 7.4. Fixed tissue was cut into 80 µm-thick sagittal vibratome sections and post-fixed in 1% osmium tetroxide. Following alcohol dehydration, tissue sections were infiltrated with increasing concentrations of Spurr resin and then embedded flat in Aclar sheets. Regions of interest for ultrastructural analyses, including the prefrontal cortex and hippocampal CA1, were excised, and 50 nm ultrathin sections were prepared and stained with uranyl acetate and lead citrate. The material was viewed using a Thermo Fisher Talos L120C transmission electron microscope operating at 120 kV. For endosome quantification, approximately 60 EM images (17,500X) per mouse were acquired. The images contained dendritic and synaptic profiles in the proximity (within 5-10 µm) of the neuronal soma located within the pyramidal cell layer V of the pre-frontal cortex (n=7 for both non-Tg and Thy1-APPL1 mice) and CA1 of the hippocampus (n=4 for both genotypes). The average size and circumference of endosomes for each mouse genotype were determined using Fiji/ImageJ (Schindelin et al., 2012). For immunogold EM, ultrathin tissue sections were mounted on nickel grids, air-dried, and then etched for 5 minutes with 1% sodium metaperiodate in PBS. After washing with filtered double-distilled water, the ultrathin tissue sections were incubated with 1% BSA in

PBS for 2 hours, followed by overnight incubation with the combination of mouse anti-APPL1 antibody (dilution of 1:2) and rabbit anti-Rab5 antibody (dilution of 1:2) in a humidified chamber at 4 °C. These sections were incubated with gold-conjugated secondary anti-mouse (size 10 nm) and anti-rabbit (size 6 nm) antibodies for 2 hours at room temperature before imaging. For colocalization quantification, approximately 40 EM images (22,000X and 57,000X) per mouse were acquired from the pyramidal cell layer V of the pre-frontal cortex and CA1 of the hippocampus of non-Tg and Thy1-APPL1 mice (n=3 each genotype). Rab5-immunoreactive endosomes, as well as rab5/APPL1 dual-immunoreactive endosomes, were counted manually, with results presented as percentage of rab5^{+}/APPL1^{+}endosomes versus total rab5^{+} endosomes.

2.7. Synaptosome isolation.

Synaptosomes were isolated from non-Tg and Thy1-APPL1 mouse hippocampi and cortex (n=6 mice per genotype). For hippocampal synaptosomes, hippocampi were homogenized in 250 µl homogenization buffer (0.32 mol/L sucrose, 0.1 mmol/L $CaCl_2$, 1 mmol/L $MgCl_2$ with protease and phosphatase inhibitors (5 µg/ml Pepstatin A, 5 µM Leupeptin, 1mM AEBSF, 1 µg/ml microcystin) as previously described (Louneva et al., 2008; Pensalfini et al., 2020). Samples were adjusted to contain 1.25 M sucrose and sequentially overlaid with 1.0 M sucrose solution containing 0.1 mM $CaCl_2$, followed by a layer of homogenization buffer. Tubes were centrifugated at 100,000 x g (32,500 RPM) for 3 hours at 4°C using a SW55Ti rotor (Beckman Coulter). Synaptosomes enriched in the interface between 1.0-1.25 M sucrose were collected and diluted with ice-cold 0.1 mM $CaCl_2$, followed by centrifugation at 50,000x g (28,000 RPM) for 30 minutes at 4°C in the SW55Ti rotor. The pellets then were washed again with 0.1 mM $CaCl_2$ and centrifuged again. Pellets were dissolved in 8M Urea prior to further biochemical analyses.

2.8. Synaptic vesicle endocytosis.

Half of the synaptosomes from non-Tg and Thy1-APPL1 mouse hippocampi (n=4 mouse each genotype) were used for synaptic vesicle endocytosis analysis (Daniel et al., 2012; Sellgren et al., 2019; Shekarabi et al., 2019). Synaptosomes from the 1.0-1.25 M sucrose interface were resuspended in sucrose/EDTA/Tris buffer (SET buffer: 0.32 M sucrose, 1 mM EDTA, 5 mM Tris (pH 7.4)) and centrifugated at 20,000 x g for 10 minutes at 4°C in a SW55Ti rotor, followed by resuspension in SET buffer. The resuspended synaptosomes were slowly frozen with 5% DMSO in SET buffer to preserve integrity as described (Daniel et al., 2012). On the day of the assay, aliquots of synaptosomes were thawed in a 37°C water bath for 80 seconds and mixed with 1 ml of ice-cold SET buffer, followed by centrifugation at 18,900 x g for 2 minutes at 4°C to pellet the synaptosomes. The synaptosome pellets were again suspended in 300 µl of SET buffer with a wide-orifice 1 ml pipette tip, followed by protein quantification. 2 µg of synaptosomes per well were loaded into 96-well polyethyleneimine coated glass microplates. 250 µM dithiothreitol was added to synaptosomes to prevent clumping. The 96-well plate with synaptosomes was then centrifugated in a microplate centrifuge (Sigma, 4-15C) at 1,500 x g for 30 minutes at 4°C to seed the synaptosomes onto the plate followed by incubation in HBK buffer (HEPES-buffered Krebs-like buffer; 143 mM NaCl, 4.7 mM KCl, 1.3 mM $MgSO_4$, 1.2 mM $CaCl_2$, 20 mM HEPES, 0.1 mM NaH_2PO_4 and 10 mM D-glucose, pH 7.4) at 37°C for 15 minutes. The synaptosomes were labelled with 5 µM of CellTracker™ Green CMFDA (5-chloromethyl fluorescein diacetate; Thermo Fisher; Cat# C7025) for 30 minutes at 37°C as an internal control dye marker, followed by 8-minutes pulse with 4 µM of the endocytic dye FM™4-64 (*N*-(3-Triethylammoniumpropyl)-4-(6-(4-(Diethylamino) Phenyl) Hexatrienyl) Pyridinium Dibromide, Thermo Fisher; T13320). Labelled synaptosomes were then washed with 1 mM of Advasep-7 (Biotium, 70029) for 2 minutes to remove extracellular dye, and fixed with 2% PFA in HBK buffer for 30 minutes on ice, followed by imaging at 40X magnification (with additional 3X zoom) using LSM880 confocal microscope. CMFDA labeling was used as an internal control to identify and segment viable synaptosomes.

From each mouse, 25 synaptosome images were taken and the intensity of FM^{TM}4-64 and CMFDA within synaptosomes were measured with Cell Profiler (https://cellprofiler.org). The ratio of FM^{TM}4-64/CMFDA per synaptosome was quantified for comparison between non-Tg and Thy1-hAPPL1 mice. Additional immunofluorescence staining with rab5 antibody (Abcam, 1:200) was done after CMFDA intake, with care to avoid dislodging the attached synaptosomes.

2.9. Novel Object Recognition.

Novel object recognition was performed according to previous publications (Pensalfini et al., 2020; Jiang et al., 2022). A multiple unit open field with four activity chambers and a digital video camera were used to record the activity of the mice inside each chamber. 12-13 month-old non-Tg and Thy1-APPL1 mice (n=10 for both genotypes) were used for the test. Habituation where the mice were allowed to freely explore the open field occurred for 5 minutes x 2 over two days. At day three, the training session was conducted by placing individual mouse with two identical objects (familiar) for 10 minutes, and then after three hours interval, with one familiar and one novel object for 10 minutes. The videos were analysed with CowLog 3 (Hänninen and Pastell, 2009) to determine the exploration time of each mouse. The results were presented as Recognition Index (RI), defined as time exploring the novel object versus sum of time exploring both the novel and familiar objects as previous described (Pensalfini et al., 2020; Jiang et al., 2022).

2.9. Experimental Design and Statistical Analysis.

All quantitative data were subjected to a two-tailed unpaired Student's t-test for a single comparison and a one-way ANOVA analysis for multiple comparisons, with post-hoc Tukey's analysis, using GraphPad Prism 8.0.1. Data is represented in bar graphs of the mean ± SEM, with individual data points for each mouse in the study group. Statistical significance is represented by asterisks: *$p<0.05$, **$p<0.01$, ***$p<0.001$. Sample sizes were determined based

on similar experimental procedures in our previous studies (Pensalfini et al., 2020; Jiang et al., 2022). Initial age-studies showed that the BFCN loss in the Thy1-APPL1 mice was first apparent at 12-13 months of age; therefore, the presented findings are of non-Tg and Thy1-hAPPL1 mice at age of 12-13 month.

3. Results

3.1. Characterization of APPL1 overexpression in the brains of transgenic mice.

APPL1 transgenic lines under the Thy1 promoter were generated, and an experimental line was chosen and backcrossed prior to expansion and experimentation (Thy1-APPL1). APPL1 overexpression was confirmed by Western blot analysis (Fig. 1A). Greater APPL1 immunolabeling was seen broadly in multiple brain regions (including cortex, hippocampus, cerebellum) when comparing Thy1-APPL1 with non-Tg mice (Fig. 1A-B), with a neuronal expression pattern evident by immunolabeling (Fig.1B-C; cortex and hippocampus). Western bot analysis of brain cortex homogenate across three age cohorts ranging from 4-5 to 12-13 months of age showed an approximate doubling of brain APPL1 levels in the Thy1-APPL1 mice compared to non-Tg littermates (Fig. 1D-E; n=3-5 for non-Tg and Thy1-APPL1; $t(6)=4.550$, $p=0.00392$ for 4-5 month-old mice; $t(6)=11.5$, $p=0.000025$ for 7-9 month-old mice; $t(6)=6.387$, $p=0.000693$ for 12-13 month-old mice; Two-tailed, unpaired t-test). Detected with a pan-rab5 antibody that does not differentiate active from inactive form of the protein, rab5 protein levels in brain homogenates were unchanged when comparing APP1 overexpressing mice to non-Tg littermates (Fig. 1D-E). Thus, Thy1-APPL1 mice show moderate APPL1 overexpression across many brain regions, an increase that does not result in a change in overall brain rab5 protein levels

3.2. Thy1-APPL1 transgenic mice have early endosomal abnormalities.

Our previous study showed that APPL1 is a molecular intermediary between APP-βCTF-driven endosomal alterations and rab5, necessary for such early endosome dysfunctions

as enlargement and disrupted trafficking resulting from increased APP-βCTF levels in a cell model (Kim et al., 2016). One goal of the current study using the Thy1-APPL1 mice was to determine whether an increase in APPL1 is sufficient to drive the same range of early endosome pathologies *in vivo*, directly testing whether APPL1 can play a primary role in AD-relevant early endosomal alterations. Immunolabeling with an anti-rab5 antibody that only detects the active, early endosome-membrane associated, GTP-bound state of rab5 (rab5-GTP) (Mani et al., 2016; Pensalfini et al., 2020) was done comparing cortical pyramidal neurons between Thy1-APPL1 and non-Tg mice (Fig. 2A). A significantly higher level of active rab5 immunolabeling was seen in cortical layer V neurons of Thy1-APPL1 mice compared to non-Tg littermates (Fig. 2A-B). Representative immunolabeling comparing 12-month-old mice is shown in Fig. 2A (with APPL1 co-immunolabeling), and quantitative data across the life-span summarized in Fig. 2B. (n=3-6 each age and genotype; $t(4)=2.844$, $p=0.0467$; $t(4)=4.467$, $p=0.0111$ for size and area of 7-9 month-old mice, respectively; $t(6)=4.614$, $p=0.00364$; $t(4)=4.930$, $p=0.00363$ for size and area of 12-13 month-old mice; $t(10)=2.515$, $p=0.0306$; $t(10)=3.737$, $p=0.00386$; $t(10)=9.818$, $p=0.000002$; for number, size and area of 22-23 month-old mice; Two-tailed, unpaired t-test). Interestingly, the youngest age group (4-5 month-old) Thy1-APPL1 mice did not show an increase in rab5-GTP early endosome number or size compared to non-Tg littermates, although APPL1 is overexpressed at this age (Fig. 1). While early endosome size and, correspondingly, early endosome area/cell were increased in all of the older groups, the number of early endosomes was not found to be increased until the oldest cohort (Fig.2B). Age-dependent endosome alterations were also observed in APOE4 mice (Nuriel et al., 2017), suggesting that endosome homeostasis may be maintained in younger mice despite a perturbation that can ultimately drive endosomal dysfunction as the brain ages. There was also significantly higher colocalization of APPL1 with rab5-GTP in Thy1-APPL1at age of 12-13 month, with Pearson's R=0.161 in non-Tg vs R=0.303 in Thy1-APPL1 mice (n=4

each for non-Tg and Thy1-APPL1 mice, *t(6)=3.986, p=0.0072*, Two-tailed, unpaired t-test), consistent with overexpressed APPL1 leading to the recruitment of rab5 to early endosomes.

The endosomal enlargement due to APPL1 overexpression was confirmed by electron microscopy (EM) in 12-13 month-old Thy1-APPL1 compared to non-Tg mice, where both endosomal size and circumference were significantly increased in layer V cells of prefrontal cortex (Fig. 2C, 2E; n=7 for non-Tg and Thy1-APPL1 mice, *t(12)=3.64, p=0.0034*; *t(12)=4.239, p=0.0012* for size and circumference, respectively; Two-tailed, unpaired t-test) and CA1 region of the hippocampus (Fig. 2D-E; n=4 for non-Tg and Thy1-APPL1 mice, *t(6)=3.327, p=0.0173*; *t(6)=3.83, p=0.00866* for size and circumference, respectively; Two-tailed, unpaired t-test). Increased association of APPL1 to rab5-positive endosomes has been previously shown in cortical neurons from both AD and DS human brain (Kim et al., 2016), consistent with an increased co-localization of APPL1 and rab5 in the Thy1-APPL1 mice (Fig. 2A). To further substantiate this co-localization at the early endosome, we performed immuno-EM of cortical and CA1 hippocampal brain sections of 12-13 month-old mice using a rabbit anti-rab5 and a murine anti-APPL1 antibody, followed by species-specific gold-conjugated secondary antibodies (anti-rabbit, 6 nm, green colored; anti-mouse, 10 nm, red colored). EM images from fields containing dendritic profiles were collected and the number of gold-particle-positive endosomal vesicles were manually counted. The ratio of rab5/APPL1 double-positive endosomes vs. total rab5 positive endosomes was significantly higher in Thy1-APPL1 compared to non-Tg mice in both brain regions (Fig. 2F-G; n=3 for non-Tg and Thy1-APPL1 mice, *t(4)=3.492, p=0.0251*; *t(4)=2.825, p=0.0476* for cortex and CA1, respectively; Two-tailed, unpaired t-test).

3.3. Endocytic abnormalities in hippocampal synaptosomes of Thy-APPL1 mice.

Given that our previous studies demonstrated that rab5 hyper-activation leads to synaptic dysfunction and deficits in memory and learning (Kaur et al., 2014; Jiang et al., 2016;

Pensalfini et al., 2020) and that endocytic activity plays a critical role in synaptic function (Overhoff et al., 2021), we sought to confirm that the overexpression of APPL1 in the Thy1-APPL1 mouse leads to differences in endosomal proteins and endocytic function in isolated synaptosomes. Synapse enrichment was confirmed by the higher level of synaptophysin in the synaptosome preparations compared to hippocampal homogenates independent of genotype (Fig. 3A and additional data not shown; n=6 per genotype, at the age of 12-13 months). While APPL1 levels were higher in the homogenates prepared from Thy1-APPL1 mice (as shown previously; Fig. 1D), the increase in APPL1 protein in the synaptosomes prepared from Thy1-APPL1 mice was found to be greater (Fig. 3A-B, 3.9-times non-Tg in synaptosomes compared to 1.9-times in homogenate, n=6, $t(10)=5.36, p=0.000319,$ Two-tailed, unpaired t-test). Total rab5 protein levels in both homogenates (see Fig. 1E) and synaptosomes were unaffected by APPL1 overexpression. While APP-βCTF levels were similar in Thy1-APPL1 and non-Tg mouse brain homogenate, APPL1 overexpression led to an increase in APP-βCTF levels within synaptosomes (Fig. 3A-B; n=6 per genotype; $t(10)=3.054, p=0.0122$; Two-tailed, unpaired t-test). Given that the APP-βCTF is the immediate precursor of Aβ, we determined brain Aβ levels using a sandwich ELISA that detects the endogenous, murine Aβ (Morales-Corraliza et al., 2009; Jiang et al., 2016) in 7-9 and 12-13 month-old mice. The levels of brain Aβ40 and Aβ42 were unchanged when comparing Thy1-APPL1 to non-Tg mice brain homogenate (data not shown).

Phosphorylated tau (identified with PHF1) (Pensalfini et al., 2020) was also increased in hippocampal synaptosomes of Thy1-APPL1 mice compared to non-Tg controls (Fig. 3A and 3C; n=6 for per genotype; $t(10)=2.922, p=0.0152$ for synaptosome PHF1; $t(10)=2.309, p=0.0436$ for PHF1/total tau in brain homogenate; $t(10)=2.432, p=0.0353$ for PHF1/total tau in synaptosome homogenate; Two-tailed, unpaired t-test), an increase in PHF1-reactivity comparable to the increase seen following neuronal rab5 overexpression (Pensalfini et al.,

2020). These findings in the Thy1-APPL1 mouse further prove that endosomal pathway disruption can contribute to tau pathobiology in AD (Knopman et al., 2021).

To directly investigate whether endocytosis was altered by the increase in APPL1 expression in the Thy1-APPL1 mice, total synaptosomes were labeled with the fluorescent dye CMFDA (Daniel et al., 2012; Sellgren et al., 2019). *Ex vivo* synaptosome endocytic uptake was determined using a second fluorescent marker, F4-64, following its internalization (Daniel et al., 2012; Sellgren et al., 2019). Confocal images of both F4-64 and CMFDA were collected and the ratios of F4-64 to CMFDA in synaptosome were quantified. A significantly greater ratio of F4-64/CMFDA was observed in hippocampal synaptosomes of Thy1-APPL1 compared to non-Tg mice at 12 months of age (Fig. 3D-E, n=4 for non-Tg and Thy1-APPL1 mice; $t(6)=2.886, p=0.0278;$ Two-tailed, unpaired t-test), while the ratios of F4-64/CMFDA remain unchanged between non-Tg and Thy-APPL1 mice at the age of 7 months (Fig. 3E, n=6; $t(10)=1.294, p=0.225;$ Two-tailed, unpaired t-test). In parallel, as determined by immunocytochemistry using an anti-rab5 antibody (Abcam, 1;200), a significantly higher ratio of rab5/CMDFA was also found in Thy1-APPL1 mice at the age of 12 months (Fig. 5F-G, n=3 for non-Tg and Thy-hAPPL1 mice; $t(4)=3.403, p=0.0272;$ Two-tailed, unpaired t-test), supporting the idea that rab5 recruitment in the Thy1-APPL1 mouse leads to greater endocytosis. These findings support our hypothesis that APPL1 acts as a molecular interface connecting rab5 and APP-βCTFs at the early endosome.

3.4. Loss of BFCNs in Thy1-APPL1 mice.

Neuronal endosomal dysfunction drives the loss of cholinergic neurons in the MSN due to a loss of trophic support mediated by signaling endosomes (Salehi et al., 2003; Howe and Mobley, 2004; Jiang et al., 2016; Chen and Mobley, 2019; Pensalfini et al., 2020; Jiang et al., 2022). Consistent with the endosomal alterations seen in the Thy1-APPL1 model, the number of ChAT-immunoreactive neurons in the MSN of Thy1-APPL1 mice showed an age-dependent loss compared to non-Tg mice (Fig. 4A-B, n=42 for total of non-Tg mice and n=41 for total of

Thy1-APPL1 mice; *F(1, 55)=6.01, p=0.017, Linear regression)*, with reduced numbers of cholinergic neurons first detected at 12 months of age (Fig. 4C, *t(25)=2.316, p=0.0291 for 12-13 month old mice*; *t(7)=2.399, p=0.0475 for 18 month old mice; t(9)=3.482, p=0.00692* for mice over 23 month old; Two-tailed, unpaired t-test). Abnormal, tortuous proximal dendrites and shrunken cholinergic cell soma (Fig. 4D, arrowheads) were also seen in the MSN neurons of aged Thy1-APPL1 compared to non-Tg mice (18 month), as has been reported in multiple AD-like models with endosomal alterations (Cataldo et al., 2000; Cataldo et al., 2003; Salehi et al., 2006; Choi et al., 2009; Jiang et al., 2016; Pensalfini et al., 2020; Jiang et al., 2022). Fig. 4E-F shows representative images of immunolabeling rab5-positive early endosomes within cholinergic neurons in a Thy1-APPL1 compared to a non-Tg mouse, both at 18-months of age. Enlarged early endosomes were apparent in the ChAT-immunoreactive cholinergic neurons of the Thy1-APPL1 mouse relative to the non-Tg littermate.

3.5. Hippocampal synaptic plasticity impairments in Thy1-hAPPL1 mice.

Alteration of hippocampal synaptic plasticity has been shown in AD-related mouse models (Marchetti and Marie, 2011; Dietrich et al., 2018), and APPL1 has been shown to be a regulator of hippocampal synaptic plasticity (Fernandez-Monreal et al., 2016; Wang et al., 2016; Formolo et al., 2022; Hua et al., 2023). We have also previously demonstrated that overactivation of rab5 resulting from neuronal rab5 overexpression leads to hippocampal-dependent memory deficits (Pensalfini et al., 2020). Long-lasting changes in synaptic plasticity measured as LTP and LTD are key mechanisms upon which learning and long-term memory are built (Avchalumov and Mandyam, 2021). Greater rab5 activation has been linked with both LTP deficit (Pensalfini et al., 2020) and LTD impairments (Hausser and Schlett, 2019; Pensalfini et al., 2020). To determine whether APPL1 overexpression in the Thy1-APPL1 mouse altered hippocampal plasticity, we measured CA1 LTP and LTD using hippocampal slices comparing Thy1-APPL1 and non-Tg mice (Fig. 5; n=5 for both genotypes at ages 7-9 and 12-13 months). In the younger age cohort (7-9 months), Thy1-APPL1 mice did not show

differences compared to non-Tg in LTP following TBS stimulation (Fig. 5A-C). However, we found a significant LTP impairment in 12-13 month-old Thy1-APPL1 mice (Fig. 5E: ($F(1, 236)=6.696, p=0.0103$ for the slope, Linear regression) and Fig. 5F: ($t(8)=2.565, p=0.0334$ for 1 minute time point; $t(8)=3.237, p=0.0237$ for 40 minutes time point; $t(8)=3.722, p=0.0175$ for 80 minutes time point; Two-tailed, unpaired multiple t-test), without apparent difference in their basal neurotransmission between the genotypes (Fig. 5D). Furthermore, post-synaptic potential (fEPSP) slopes indicated suppressed LTD upon induction by LSF (1 Hertz for 900 seconds) in 12-13 month-old Thy1-APPL1 mice compared to their age-matched non-Tg littermates (Fig. 5H: ($F(1, 127)=14.83, p=0.0002$ for the intercepts, Linear regression and Fig. 5I: ($t(8)=5.277, p=0.000749$ for 50 minutes time point; Two-tailed, unpaired t-test). Thus, we show both loss of BFCNs as well as disruption of hippocampal LTP and LDP as the Thy1-APPL1 mice age. Consistent with these electrophysiological findings, hippocampal-dependent memory assessed by Novel Object Recognition (NOR) showed impairment in Thy1-APPL1 mice at 12-13 months of age (Fig. 5J; n=10 for non-Tg and Thy1-APPL1 mice; $t(18)=2.187, p=0.042$; Two-tailed, unpaired t-test)

4. Discussion

Endosomal pathway dysfunction within neurons is one of the earliest pathologies of Alzheimer's disease, with endosomal enlargement occurring years, even decades, prior to β-amyloid plaques accumulation and PHF tau tangles (Cataldo et al., 1996; Cataldo et al., 2000; Nixon, 2017). Increased APP-βCTF levels cause enlargement of early endosomes and degeneration of BFCNs in Down syndrome mouse models (Jiang et al., 2016; Jiang et al., 2022) and impaired trophic function via retrogradely transported signaling endosomes (Salehi et al., 2006; Xu et al., 2016). Both APP-βCTFs and APPL1 are elevated in human AD brain (Kim et al., 2016; Johnson et al., 2022), and extensive evidence shows that APPL1 mediates APP-βCTF-endosome signaling. Over-expressed APPL1 binds to APP-βCTFs, altering early endosome size and function (Kim et al., 2016). By contrast, downregulation of APPL1 by siRNA has the opposite effects on endosomes (Kim et al., 2016). In DS fibroblasts, which have enlarged early endosomes due to increased APP-βCTF levels, treating with siRNA to reduce APPL1 levels restored early endosome morphology and function to that seen in diploid cells (Kim et al., 2016).

Given the prominence of early endosome alterations in early AD and our previous findings showing that APPL1 acts as the molecular intermediary linking rab5 activation and endosomal pathology to increased endolysosomal APP-βCTF levels in multiple APP over-expression systems (Kim et al., 2016), we undertook this study to further dissect APPL1's roles *in vivo*. APPL1 was previously shown using *in vitro* models to be necessary for the APP-βCTF-mediated increase in rab5 activity, accelerated endocytosis, and selective impairment of axonal transport of endosomes in neuronal cells by stabilizing the active rab5-GTP complex (Kim et al., 2016). With APPL1 expression in the brain approximately doubled in the Thy1-APPL1 mice, we were able to directly examine *in vivo* the ability of APPL1 to mediate the diverse early endosome pathologies previously reported following APP-βCTF accumulation or rab5

overactivity (Cataldo et al., 1997; Jiang et al., 2016; Kim et al., 2016; Pensalfini et al., 2020). APPL1 overexpression in neurons resulted in higher levels of rab5 activation as shown by enlarged neuronal rab5-GTP-positive endosomes and altered ultrastructural endosomal morphology (Fig. 2), an AD-related endosomal phenotype that is associated with multiple endolysosomal and neurodegenerative phenotypes (Nixon et al., 2017; Colacurcio et al., 2018; Mathews and Levy, 2019). As one would predict, given the prominent early endosome alterations seen in Thy1-APPL1 mouse neurons, we saw aging-dependent loss of BFCNs, a phenotype seen in AD models that recapitulate early endosome dysfunction (Cataldo et al., 1997; Jiang et al., 2016; Kim et al., 2016; Pensalfini et al., 2020). In the Thy1-APPL1 model, early endosome alterations and these downstream effects were aging-dependent, with enlarged early endosomes (detected initially at 7-9 months of age) seen prior to BFCN loss (12-13 months of age). Additionally, changes in LTP and LDP were aging-dependent and initially detected later (at 12-13 months of age) than the age when early endosome enlargement in cortical neurons was first seen, suggesting that the impact of the loss of efficient trophic support mediated by dysfunctional signaling endosomes plays out over time. Indeed, mouse models typically show BFCN degeneration months following detectable endosomal alterations (Cataldo et al., 2000; Cataldo et al., 2003; Salehi et al., 2006; Choi et al., 2009; Jiang et al., 2016; Pensalfini et al., 2020; Jiang et al., 2022). That neuronal early endosome enlargement in the Thy1-APPL1 mouse is not seen at 4-5 months of age but detected later is consistent with other models in which the neuronal early endosome appears to be resilient in the younger brain, while this homeostatic ability is lost during aging (Nuriel et al., 2017; Mathews and Levy, 2019). Interestingly, in a model with direct rab5 overactivation (Pensalfini et al., 2020), loss of endosomal homeostasis is apparent early, suggesting that regulatory mechanisms more distant from rab5, albeit capable of driving endosomal dysfunction through rab5 overactivation, may be tolerated until the brain begins to age.

Additionally, phosphorylated tau, as detected by PHF1, was increased in synaptosomes isolated from the Thy1-APPL1 mice (Fig. 3). Endosomal pathway function is known to impact tau phosphorylation as well as the spread and seeding of pathogenic tau within the brain (Knopman et al., 2021). APPL1 kinase-signaling is also likely to affect tau phosphorylation directly in the Thy1-APPL1 model (Diggins and Webb, 2017), with APPL1 modulating the phosphorylation of GSK3β through its interaction with Akt (Mitsuuchi et al., 1999).

Rab5 is associated with both pre- and post-synaptic vesicles, where rab5 is critical in mediating function by regulating synaptic vesicle endocytosis and thus membrane and protein cargo retrieval (Star et al., 2005; Chanaday et al., 2019), functions that are vulnerable in neurodegenerative diseases (Bonnycastle et al., 2021; Harper and Smillie, 2021; Bellucci et al., 2022). Synaptosomes containing numerous synaptic vesicles have been used as an *ex vivo* system to study synaptic dysfunctions in AD and other neurodegenerative diseases (Evans, 2015; Jhou and Tai, 2017; Ahmad and Liu, 2020; Griffiths and Grant, 2023). Increased APPL1 expression results in increased synaptosome endocytosis (Fig. 3D-E), consistent with increased active rab5 on neuronal endosomes (Fig. 2A-B). Both knockdown mediated by siRNA and an APPL1 functional knockdown mediated by inhibitory peptides have shown that APPL1 is necessary for normal hippocampal synaptic plasticity (Fernandez-Monreal et al., 2016; Wang et al., 2016; Wu et al., 2020; Formolo et al., 2022; Hua et al., 2023). APPL1 overexpression produced similar LTP and LTD results to those seen in previous studies with APPL1 down regulation (Fernandez-Monreal et al., 2016; Wu et al., 2020). Nevertheless, given APPL1's functions at the early endosome, both under and overexpression of APPL1 are likely to perturb early endosome signaling as well as the formation and cargo-acquisition of early endosomes through endocytosis (Diggins and Webb, 2017). Overexpression of APPL1 in the Thy1-APPL1 mouse increased rab5 activity, driving synaptic endocytosis. It is also likely to lead to entrapment of endocytic cargo, which enlarges early endosomes preventing appropriate

synaptic vesicle recycling and trafficking. The increase of APP-βCTFs seen in the synaptosomes of Thy1-APPL1 mouse is also consistent with endocytosed cargo being entrapped in early endosomes. BACE1 cleavage of APP to generate APP-βCTFs occurs in endocytic compartments, and increasing the uptake and dwell-time of APP within endosomes increases APP-βCTF generation (De Strooper and Karran, 2016). Abundant APPL1 at endosomes, given its interaction with endosomal APP-βCTFs, is likely to increase the dwell time of the APPL1/APP-βCTF complex, further accentuating downstream signaling to rab5.

In addition to its various neuronal signaling functions (Lin et al., 2006; Deepa and Dong, 2009; Lee et al., 2011; Hupalowska et al., 2012), APPL1 acts as a molecular link between APP-βCTF and rab5 (Kim et al., 2016), a critical cross-roads for pathways that converge on the early endosome during AD pathobiology. The Thy1-APPL1 mouse validates the importance of normal APPL1 function to neuronal function and viability; and highlights the important role APPL1 plays in transducing APP-βCTF-signaling in AD to rab5, thus regulating early endosome function. That increased APP-βCTFs lead to early endosomal changes has been established through multiple experimental systems (Cataldo et al., 2003; Salehi et al., 2006; Jiang et al., 2016; Kim et al., 2016). We now show that overexpression of APPL1 leads to similar phenotypes that are also achieved by the direct overactivation of rab5 (Pensalfini et al., 2020). Whether other risk factors for AD-driven early endosome and synaptic dysfunction, such as APOE4, BIN1, CD2AP, PICAM, RIN3, SORL1 and others (Nixon, 2017; Perdigão et al., 2020) can act through APPL1 is unknown; nevertheless, the Thy1-APPL1 model further demonstrates that multiple molecular mechanisms leading to AD-like early endosome dysfunction are known to converge on rab5 and its regulation.

References.

Ahmad F, Liu P (2020) Synaptosome as a tool in Alzheimer's disease research. Brain Res 1746:147009.

Avchalumov Y, Mandyam CD (2021) Plasticity in the Hippocampus, Neurogenesis and Drugs of Abuse. Brain Sci 11.

Bellucci A, Longhena F, Spillantini MG (2022) The Role of Rab Proteins in Parkinson’s Disease Synaptopathy. Biomedicines 10:1941.

Bohdanowicz M, Balkin DM, De Camilli P, Grinstein S (2012) Recruitment of OCRL and Inpp5B to phagosomes by Rab5 and APPL1 depletes phosphoinositides and attenuates Akt signaling. Mol Biol Cell 23:176-187.

Bonnycastle K, Davenport EC, Cousin MA (2021) Presynaptic dysfunction in neurodevelopmental disorders: Insights from the synaptic vesicle life cycle. Journal of Neurochemistry 157:179-207.

Bourgeois A, Lauritzen I, Lorivel T, Bauer C, Checler F, Pardossi-Piquard R (2018) Intraneuronal accumulation of C99 contributes to synaptic alterations, apathy-like behavior, and spatial learning deficits in 3xTgAD and 2xTgAD mice. Neurobiol Aging 71:21-31.

Cataldo AM, Barnett JL, Pieroni C, Nixon RA (1997) Increased neuronal endocytosis and protease delivery to early endosomes in sporadic Alzheimer's disease: neuropathologic evidence for a mechanism of increased beta-amyloidogenesis. J Neurosci 17:6142-6151.

Cataldo AM, Hamilton DJ, Barnett JL, Paskevich PA, Nixon RA (1996) Abnormalities of the endosomal-lysosomal system in Alzheimer's disease: relationship to disease pathogenesis. Adv Exp Med Biol 389:271-280.

Cataldo AM, Peterhoff CM, Troncoso JC, Gomez-Isla T, Hyman BT, Nixon RA (2000) Endocytic pathway abnormalities precede amyloid beta deposition in sporadic

Alzheimer's disease and Down syndrome: differential effects of APOE genotype and presenilin mutations. Am J Pathol 157:277-286.

Cataldo AM, Petanceska S, Peterhoff CM, Terio NB, Epstein CJ, Villar A, Carlson EJ, Staufenbiel M, Nixon RA (2003) App gene dosage modulates endosomal abnormalities of Alzheimer's disease in a segmental trisomy 16 mouse model of down syndrome. J Neurosci 23:6788-6792.

Chanaday NL, Cousin MA, Milosevic I, Watanabe S, Morgan JR (2019) The Synaptic Vesicle Cycle Revisited: New Insights into the Modes and Mechanisms. The Journal of Neuroscience 39:8209-8216.

Chen XQ, Mobley WC (2019) Exploring the Pathogenesis of Alzheimer Disease in Basal Forebrain Cholinergic Neurons: Converging Insights From Alternative Hypotheses. Front Neurosci 13:446.

Choi JH, Kaur G, Mazzella MJ, Morales-Corraliza J, Levy E, Mathews PM (2013) Early endosomal abnormalities and cholinergic neuron degeneration in amyloid-beta protein precursor transgenic mice. J Alzheimers Dis 34:691-700.

Choi JH, Berger JD, Mazzella MJ, Morales-Corraliza J, Cataldo AM, Nixon RA, Ginsberg SD, Levy E, Mathews PM (2009) Age-dependent dysregulation of brain amyloid precursor protein in the Ts65Dn Down syndrome mouse model. J Neurochem 110:1818-1827.

Colacurcio DJ, Pensalfini A, Jiang Y, Nixon RA (2018) Dysfunction of autophagy and endosomal-lysosomal pathways: Roles in pathogenesis of Down syndrome and Alzheimer's Disease. Free Radic Biol Med 114:40-51.

Daniel JA, Malladi CS, Kettle E, McCluskey A, Robinson PJ (2012) Analysis of synaptic vesicle endocytosis in synaptosomes by high-content screening. Nat Protoc 7:1439-1455.

De Strooper B, Karran E (2016) The Cellular Phase of Alzheimer's Disease. Cell 164:603-615.

Deepa SS, Dong LQ (2009) APPL1: role in adiponectin signaling and beyond. Am J Physiol Endocrinol Metab 296:E22-36.

Dietrich K, Bouter Y, Müller M, Bayer TA (2018) Synaptic Alterations in Mouse Models for Alzheimer Disease—A Special Focus on N-Truncated Abeta 4-42. Molecules 23:718.

Diggins NL, Webb DJ (2017) APPL1 is a multifunctional endosomal signaling adaptor protein. Biochem Soc Trans 45:771-779.

Evans GJ (2015) The synaptosome as a model system for studying synaptic physiology. Cold Spring Harb Protoc 2015:421-424.

Fahimi A, Noroozi M, Salehi A (2021) Chapter 13 - Enlargement of early endosomes and traffic jam in basal forebrain cholinergic neurons in Alzheimer's disease. In: Handbook of Clinical Neurology (Swaab DF, Kreier F, Lucassen PJ, Salehi A, Buijs RM, eds), pp 207-218: Elsevier.

Fernandez-Monreal M, Sanchez-Castillo C, Esteban JA (2016) APPL1 gates long-term potentiation through its plekstrin homology domain. J Cell Sci 129:2793-2803.

Formolo DA, Cheng T, Yu J, Kranz GS, Yau S-Y (2022) Central Adiponectin Signaling – A Metabolic Regulator in Support of Brain Plasticity. Brain Plasticity 8:79-96.

Goto-Silva L, McShane MP, Salinas S, Kalaidzidis Y, Schiavo G, Zerial M (2019) Retrograde transport of Akt by a neuronal Rab5-APPL1 endosome. Scientific Reports 9:2433.

Griffiths J, Grant SGN (2023) Synapse pathology in Alzheimer's disease. Seminars in Cell & Developmental Biology 139:13-23.

Hänninen L, Pastell M (2009) CowLog: Open-source software for coding behaviors from digital video. Behavior Research Methods 41:472-476.

Harper CB, Smillie KJ (2021) Current molecular approaches to investigate pre-synaptic dysfunction. Journal of Neurochemistry 157:107-129.

Hausser A, Schlett K (2019) Coordination of AMPA receptor trafficking by Rab GTPases. Small GTPases 10:419-432.

Howe CL, Mobley WC (2004) Signaling endosome hypothesis: A cellular mechanism for long distance communication. J Neurobiol 58:207-216.

Hua S-S, Ding J-J, Sun T-C, Guo C, Zhang Y, Yu Z-H, Cao Y-Q, Zhong L-H, Wu Y, Guo L-Y, Luo J-H, Cui Y-H, Qiu S (2023) NMDA Receptor–Dependent Synaptic Potentiation via APPL1 Signaling Is Required for the Accessibility of a Prefrontal Neuronal Assembly in Retrieving Fear Extinction. Biological Psychiatry 94:262-277.

Hupalowska A, Pyrzynska B, Miaczynska M (2012) APPL1 regulates basal NF-kappaB activity by stabilizing NIK. J Cell Sci 125:4090-4102.

Jhou JF, Tai HC (2017) The Study of Postmortem Human Synaptosomes for Understanding Alzheimer's Disease and Other Neurological Disorders: A Review. Neurol Ther 6:57-68.

Jiang Y, Mullaney KA, Peterhoff CM, Che S, Schmidt SD, Boyer-Boiteau A, Ginsberg SD, Cataldo AM, Mathews PM, Nixon RA (2010) Alzheimer's-related endosome dysfunction in Down syndrome is Abeta-independent but requires APP and is reversed by BACE-1 inhibition. Proc Natl Acad Sci U S A 107:1630-1635.

Jiang Y, Rigoglioso A, Peterhoff CM, Pawlik M, Sato Y, Bleiwas C, Stavrides P, Smiley JF, Ginsberg SD, Mathews PM, Levy E, Nixon RA (2016) Partial BACE1 knockdown in a Down syndrome mouse model blocks Alzheimer-related endosomal anomolies and cholinergic neurodegeneration: role of APP-CTF. . Neurobiol Aging 39:8.

Jiang Y et al. (2022) Preclinical and randomized clinical evaluation of the p38alpha kinase inhibitor neflamapimod for basal forebrain cholinergic degeneration. Nat Commun 13:5308.

Johnson ECB et al. (2022) Large-scale deep multi-layer analysis of Alzheimer's disease brain reveals strong proteomic disease-related changes not observed at the RNA level. Nat Neurosci 25:213-225.

Kaur G, Sharma A, Xu W, Gerum S, Alldred MJ, Subbanna S, Basavarajappa BS, Pawlik M, Ohno M, Ginsberg SD, Wilson DA, Guilfoyle DN, Levy E (2014) Glutamatergic transmission aberration: a major cause of behavioral deficits in a murine model of Down's syndrome. J Neurosci 34:5099-5106.

Kim S, Sato Y, Mohan PS, Peterhoff C, Pensalfini A, Rigoglioso A, Jiang Y, Nixon RA (2016) Evidence that the rab5 effector APPL1 mediates APP-betaCTF-induced dysfunction of endosomes in Down syndrome and Alzheimer's disease. Mol Psychiatry.

Knopman DS, Amieva H, Petersen RC, Chételat G, Holtzman DM, Hyman BT, Nixon RA, Jones DT (2021) Alzheimer disease. Nat Rev Dis Primers 7:33.

Langemeyer L, Fröhlich F, Ungermann C (2018) Rab GTPase Function in Endosome and Lysosome Biogenesis. Trends Cell Biol 28:957-970.

Lauritzen I, Pardossi-Piquard R, Bourgeois A, Bécot A, Checler F (2019) Does Intraneuronal Accumulation of Carboxyl-terminal Fragments of the Amyloid Precursor Protein Trigger Early Neurotoxicity in Alzheimer's Disease? Curr Alzheimer Res 16:453-457.

Lauritzen I, Pardossi-Piquard R, Bourgeois A, Pagnotta S, Biferi MG, Barkats M, Lacor P, Klein W, Bauer C, Checler F (2016) Intraneuronal aggregation of the beta-CTF fragment of APP (C99) induces Abeta-independent lysosomal-autophagic pathology. Acta Neuropathol 132:257-276.

Lee JR, Hahn HS, Kim YH, Nguyen HH, Yang JM, Kang JS, Hahn MJ (2011) Adaptor protein containing PH domain, PTB domain and leucine zipper (APPL1) regulates the protein level of EGFR by modulating its trafficking. Biochem Biophys Res Commun 415:206-211.

Lin DC, Quevedo C, Brewer NE, Bell A, Testa JR, Grimes ML, Miller FD, Kaplan DR (2006) APPL1 associates with TrkA and GIPC1 and is required for nerve growth factor-mediated signal transduction. Mol Cell Biol 26:8928-8941.

Louneva N, Cohen JW, Han LY, Talbot K, Wilson RS, Bennett DA, Trojanowski JQ, Arnold SE (2008) Caspase-3 is enriched in postsynaptic densities and increased in Alzheimer's disease. Am J Pathol 173:1488-1495.

Majumdar D, Nebhan CA, Hu L, Anderson B, Webb DJ (2011) An APPL1/Akt signaling complex regulates dendritic spine and synapse formation in hippocampal neurons. Mol Cell Neurosci 46:633-644.

Mani M, Lee UH, Yoon NA, Kim HJ, Ko MS, Seol W, Joe Y, Chung HT, Lee BJ, Moon CH, Cho WJ, Park JW (2016) Developmentally regulated GTP-binding protein 2 coordinates Rab5 activity and transferrin recycling. Mol Biol Cell 27:334-348.

Marchetti C, Marie H (2011) Hippocampal synaptic plasticity in Alzheimer's disease: what have we learned so far from transgenic models? Rev Neurosci 22:373-402.

Mathews PM, Levy E (2019) Exosome Production Is Key to Neuronal Endosomal Pathway Integrity in Neurodegenerative Diseases. Front Neurosci 13:1347.

Mitsuuchi Y, Johnson SW, Sonoda G, Tanno S, Golemis EA, Testa JR (1999) Identification of a chromosome 3p14.3-21.1 gene, APPL, encoding an adaptor molecule that interacts with the oncoprotein-serine/threonine kinase AKT2. Oncogene 18:4891-4898.

Morales-Corraliza J, Mazzella MJ, Berger JD, Diaz NS, Choi JH, Levy E, Matsuoka Y, Planel E, Mathews PM (2009) In vivo turnover of tau and APP metabolites in the brains of wild-type and Tg2576 mice: greater stability of sAPP in the beta-amyloid depositing mice. PLoS One 4:e7134.

Nixon RA (2017) Amyloid precursor protein and endosomal-lysosomal dysfunction in Alzheimer's disease: inseparable partners in a multifactorial disease. FASEB J 31:2729-2743.

Nixon RA, Jiang Y, Sato Y, Im E, Bordi M, Colacurcio D, Pensalfini A, Rigoglioso A, Mohan P (2017) APP-β CTF-mediated pathological endosome signaling also disrupts lysosomal function in Down syndrome (DS). In.

Nuriel T, Peng KY, Ashok A, Dillman AA, Figueroa HY, Apuzzo J, Ambat J, Levy E, Cookson MR, Mathews PM, Duff KE (2017) The Endosomal-Lysosomal Pathway Is Dysregulated by APOE4 Expression in Vivo. Front Neurosci 11:702.

Ogawa A, Yamazaki Y, Nakamori M, Takahashi T, Kurashige T, Hiji M, Nagano Y, Yamawaki T, Matsumoto M (2013) Characterization and distribution of adaptor protein containing a PH domain, PTB domain and leucine zipper motif (APPL1) in Alzheimer's disease hippocampus: an immunohistochemical study. Brain Res 1494:118-124.

Overhoff M, De Bruyckere E, Kononenko NL (2021) Mechanisms of neuronal survival safeguarded by endocytosis and autophagy. J Neurochem 157:263-296.

Peng KY, Liemisa B, Pasato J, D'Acunzo P, Pawlik M, Heguy A, Penikalapati SC, Labuza A, Pidikiti H, Alldred MJ, Ginsberg SD, Levy E, Mathews PM (2024) Apolipoprotein E2 Expression Alters Endosomal Pathways in a Mouse Model With Increased Brain Exosome Levels During Aging. Traffic 25:e12937.

Pensalfini A, Kim S, Subbanna S, Bleiwas C, Goulbourne CN, Stavrides PH, Jiang Y, Lee JH, Darji S, Pawlik M, Huo C, Peddy J, Berg MJ, Smiley JF, Basavarajappa BS, Nixon RA (2020) Endosomal Dysfunction Induced by Directly Overactivating Rab5 Recapitulates Prodromal and Neurodegenerative Features of Alzheimer's Disease. Cell Rep 33:108420.

Pera M, Alcolea D, Sanchez-Valle R, Guardia-Laguarta C, Colom-Cadena M, Badiola N, Suarez-Calvet M, Llado A, Barrera-Ocampo AA, Sepulveda-Falla D, Blesa R, Molinuevo JL, Clarimon J, Ferrer I, Gelpi E, Lleo A (2013) Distinct patterns of APP processing in the CNS in autosomal-dominant and sporadic Alzheimer disease. Acta Neuropathol 125:201-213.

Perdigão C, Barata MA, Araújo MN, Mirfakhar FS, Castanheira J, Guimas Almeida C (2020) Intracellular Trafficking Mechanisms of Synaptic Dysfunction in Alzheimer's Disease. Front Cell Neurosci 14:72.

Salehi A, Delcroix JD, Mobley WC (2003) Traffic at the intersection of neurotrophic factor signaling and neurodegeneration. Trends Neurosci 26:73-80.

Salehi A, Delcroix JD, Belichenko PV, Zhan K, Wu C, Valletta JS, Takimoto-Kimura R, Kleschevnikov AM, Sambamurti K, Chung PP, Xia W, Villar A, Campbell WA, Kulnane LS, Nixon RA, Lamb BT, Epstein CJ, Stokin GB, Goldstein LS, Mobley WC (2006) Increased App expression in a mouse model of Down's syndrome disrupts NGF transport and causes cholinergic neuron degeneration. Neuron 51:29-42.

Schindelin J, Arganda-Carreras I, Frise E, Kaynig V, Longair M, Pietzsch T, Preibisch S, Rueden C, Saalfeld S, Schmid B, Tinevez JY, White DJ, Hartenstein V, Eliceiri K, Tomancak P, Cardona A (2012) Fiji: an open-source platform for biological-image analysis. Nat Methods 9:676-682.

Schmidt SD, Nixon RA, Mathews PM (2005) ELISA Method for Measurement of Amyloid-ß Levels. In: Amyloid Proteins: Methods and Protocols (Sigurdsson EM, ed), pp 279-297. Totowa, NJ: Humana Press.

Schmidt SD, Nixon RA, Mathews PM (2012) Tissue processing prior to analysis of Alzheimer's disease associated proteins and metabolites, including Abeta. Methods Mol Biol 849:493-506.

Sellgren CM, Gracias J, Watmuff B, Biag JD, Thanos JM, Whittredge PB, Fu T, Worringer K, Brown HE, Wang J, Kaykas A, Karmacharya R, Goold CP, Sheridan SD, Perlis RH (2019) Increased synapse elimination by microglia in schizophrenia patient-derived models of synaptic pruning. Nature Neuroscience 22:374-385.

Shekarabi M, Robinson JA, Smith MD, Burdo TH (2019) SIV-Mediated Synaptic Dysfunction Is Associated with an Increase in Synapsin Site 1 Phosphorylation and Impaired PP2A Activity. J Neurosci 39:7006-7018.

Star EN, Newton AJ, Murthy VN (2005) Real-time imaging of Rab3a and Rab5a reveals differential roles in presynaptic function. The Journal of Physiology 569:103-117.

Subbanna S, Shivakumar M, Psychoyos D, Xie S, Basavarajappa BS (2013) Anandamide-CB1 receptor signaling contributes to postnatal ethanol-induced neonatal neurodegeneration, adult synaptic, and memory deficits. J Neurosci 33:6350-6366.

Wang J, Lu W, Chen L, Zhang P, Qian T, Cao W, Luo J (2016) Serine 707 of APPL1 is Critical for the Synaptic NMDA Receptor-Mediated Akt Phosphorylation Signaling Pathway. Neurosci Bull 32:323-330.

Wu Y, Lv X, Wang H, Qian K, Ding J, Wang J, Hua S, Sun T, Zhou Y, Yu L, Qiu S (2020) Adaptor protein APPL1 links neuronal activity to chromatin remodeling in cultured hippocampal neurons. Journal of Molecular Cell Biology 13:335-346.

Xu W, Weissmiller AM, White JA, 2nd, Fang F, Wang X, Wu Y, Pearn ML, Zhao X, Sawa M, Chen S, Gunawardena S, Ding J, Mobley WC, Wu C (2016) Amyloid precursor protein-mediated endocytic pathway disruption induces axonal dysfunction and neurodegeneration. J Clin Invest 126:1815-1833.

Yang DS, Lee JH, Nixon RA (2009) Monitoring autophagy in Alzheimer's disease and related neurodegenerative diseases. Methods Enzymol 453:111-144.

Figure Legends.

Figure 1. APPL1 transgene expression in the brain.

A. Representative Western blot comparing APPL1 expression in various brain regions (CTX-cortex; HIP-hippocampus; CBL-cerebellum; RB-remaining brain) from 4–5 month-old non-transgenic littermate (non-Tg) and Thy1-APP1 transgenic (Thy1-APPL1) mice. Over-expressed flag-tagged APPL1-proteins were detected in all brain regions in Thy-APPL1 mice. ***B.*** Representative brain section immunolabeling with an anti-APPL1 antibody at low magnification (scale bar 1mm) demonstrate the APPL1 over-expression patterns in various brain regions of Thy-hAPPL1 mice. ***C.*** Representative images of low and higher magnification (scale bar, 10 µm; arrowheads indicating corresponding cells) show APPL1 staining in the cortex regions. ***D.*** Western blots of APPL1 and rab5 and ***E.*** their quantification showing increased APPL1 in the brain of Thy1-APPL1 mice versus non-Tg mice at the indicated ages. $^{**}p<0.01$, $^{***}p<0.001$, Two-tailed, unpaired t-test. Data are means ± SEMs.

Figure 2. Early endosome alterations in Thy1-APPL1 mice.

A. Representative immunofluorescent images of active, GTP-bound rab5 (rab5-GTP; red) and APPL1 (green) in neurons (layer V, pre-frontal cortex) of non-Tg and Thy1-APPL1 mouse at 12-13 months of age. Scale bar 10 µm. ***B.*** Quantification of the average number, size, and total area of Rab5-GTP immunolabeled endosomes per cortical neuron in non-Tg versus Thy1-APPL1 mice at the indicated ages. Representative electron microscopy images containing dendritic profiles in layer V of pre-frontal cortex (***C***) and hippocampus (***D***) regions, and (***E***) quantification of average size and circumference of endosomes in both cortex and hippocampi showing the enlargement in Thy1-APPL1 compared to non-Tg mice aged at 12-13 months (red asterisk indicating endosome; 7 mice each genotype for cortex and 4 mice each genotype for hippocampi were used for quantification. Scale bar, 500 nm). ***F.*** Representative immuno-electron microscopy images containing dendritic profiles in layer V of pre-frontal cortex labelled with rabbit anti-rab5 and mouse anti-APPL1 followed by gold-conjugated secondary

anti-rabbit (6 nm, green arrow) and anti-mouse (10 nm, red arrow) in non-Tg and Thy1-APPL1 mice. Scale bar 500 nm. ***G.*** Percentage of rab5/APPL1 double-positive endosomes versus total rab5-positive endosomes in the dendritic region of cortex and hippocampus significantly increased in Thy1-hAPPL1 mice. N=3 per genotype. Scale bar, 100 nm. *$p<0.05$, **$p<0.01$, ***$p<0.001$, Two-tailed, unpaired t-test. Data are means ± SEMs.

Figure 3. Western blot analysis and synaptic vesicle endocytosis (SVE) revealed the abnormalities in hippocampal synaptosomes of Thy1-APPL1 mice.

A. Representative Western blots from one of the two experiments showing various protein markers and quantitation (***B-C)*** in hippocampal homogenates and hippocampal synaptosome preparations from non-Tg and Thy-APPL1 mice (n=6 each genotype), showing significant increase of APPL1, βCTF, PHF1 and the ratio of PHF1/total tau in synaptosomes of Thy1-APPL1 compared to non-Tg mice at 12–13 months of age. ***D.*** Representative fluorescent images of F4-64 (red, labelling endocytosed vesicle) internalized through SVE by hippocampal synaptosomes and CMFDA (green, control dye for synaptosome)of non-Tg and Thy1-APPL1 mice aged 12-13 months and (***E***) the intensity ratio of F4/64 to CMDFA was significantly increased in hippocampal synaptosome of Thy1-hAPPL1 mice at 12-13 month, but not in 7 months, indicating elevated endocytosis only in older Thy1-APPL1 mice. ***F.*** Representative images of CMFDA (green) labelling followed by anti-Rab5 (red) immuno-labeling and quantification of the ratio of the intensity of Rab5 to CMFDA (***G***) showing a similar increase as the ratio of the intensity of F4-64 to CMFDA in hippocampal synaptosomes of Thy1-APPL1 mice at 12-13 months of age. Scale bar, 5 µm, *$p<0.05$, ***$p<0.001$, Two-tailed, unpaired t-test. Data are means ± SEMs.

Figure 4. Loss of cholinergic neurons in the medial septal nucleus (MSN) of Thy1-APPL1 mice.

A. Representative light microscopy images comparing ChAT immunoreactive neurons in the MSN of non-Tg and Thy1-APPL1 mice at 12-13 months of age. Scale bar, 100 µm. ***B.*** Plots

of numbers of ChAT$^+$ neurons (x1000) counted stereologically versus age of mice showing significant difference between the slopes of non-Tg and Thy1-APPL1 mice (*F(1, 55)=6.01, p=0.017,* Linear regression*)*. ***C.*** Number ChAT -immunoreactive neurons in the MSN of non-Tg and Thy1-APPL1 mice at the indicated ages (n = 42 for non-Tg and 41 for Thy1-APPL1 mice; quantitative stereology as described in Methods). ***D.*** Representative images of ChAT$^+$ neurons in higher magnifications at 18-month-old non-Tg and Thy1-APPL1 mice, with arrow heads pointing to dystrophic neurites. Scale bar, 5 µm. ***E***. Representative z-stacked series fluorescence images of ChAT- (red) and rab5-immunoreactive (green) neuron in the MSN of a non-Tg and Thy1-APPL1 mice mouse at 18 months of age, with arrows pointing to a dystrophic neurite. Scale bar 5 µm. *$p<0.05$, ***$p<0.001$, Two-tailed, unpaired t-test. Data are means ± SEMs.

Figure 5. Age- related impairments of synaptic plasticity and hippocampal-dependent memory deficit in Thy1-APPL1 mice

A-C. non-Tg and Thy1-APPL1 mice at 7-9 months of age (n=5 for both genotype), input/output relationship plots (***A***), LTP by theta-burst stimulation (TBS) in the Schaffer collateral synapses (CA3-CA1) of hippocampal slices (***B)*** and averages of fEPSP slopes at 1, 40, and 80 minutes following tetanic stimulation (***C***) of the hippocampal slices showing no differences between non-Tg and Thy1-APPL1 mice. ***D-F,*** non-Tg and Thy1-APPL1 mice at 12-13 months of age (n=5 for both genotype), input/output relationship plots (***D)***, LTP induced by TBS in the Schaffer collateral synapses (CA3-CA1) in hippocampal slices (***E***) and averages of fEPSP slopes at 1, 40, and 80 minutes (***F***) showing significant reduction in Thy1-APPL1 mice (*F(1, 236)=6.696, p=0.0103* for the slope, linear regression). ***G-I.*** non-Tg, and Thy1-APPL1 mice at 12-13 months of age, (n=5 for both genotypes), input/output relationship plots (***G***), LTD induced by low-frequency stimulation (LFS) (***H***) in hippocampal slices of Thy1-APPL1 (*F(1, 127)=14.83, p=0.0002* for the intercepts, linear regression), and averages of fEPSP slopes at 50 minutes following LFS induction (***I)*** in the hippocampal slices did not show expected

reduction in Thy1-hAPPL1 mice. (***J)*** Recognition index at 3 hours after familiarization indicated the memory deficit in Thy1-APPL1 mice at 12-13 months of age ($t(18)=2.187$, $p=0.042$). *$p<0.05$, ***$p<0.001$, Two-tailed, unpaired t-test. Data are means ± SEMs.

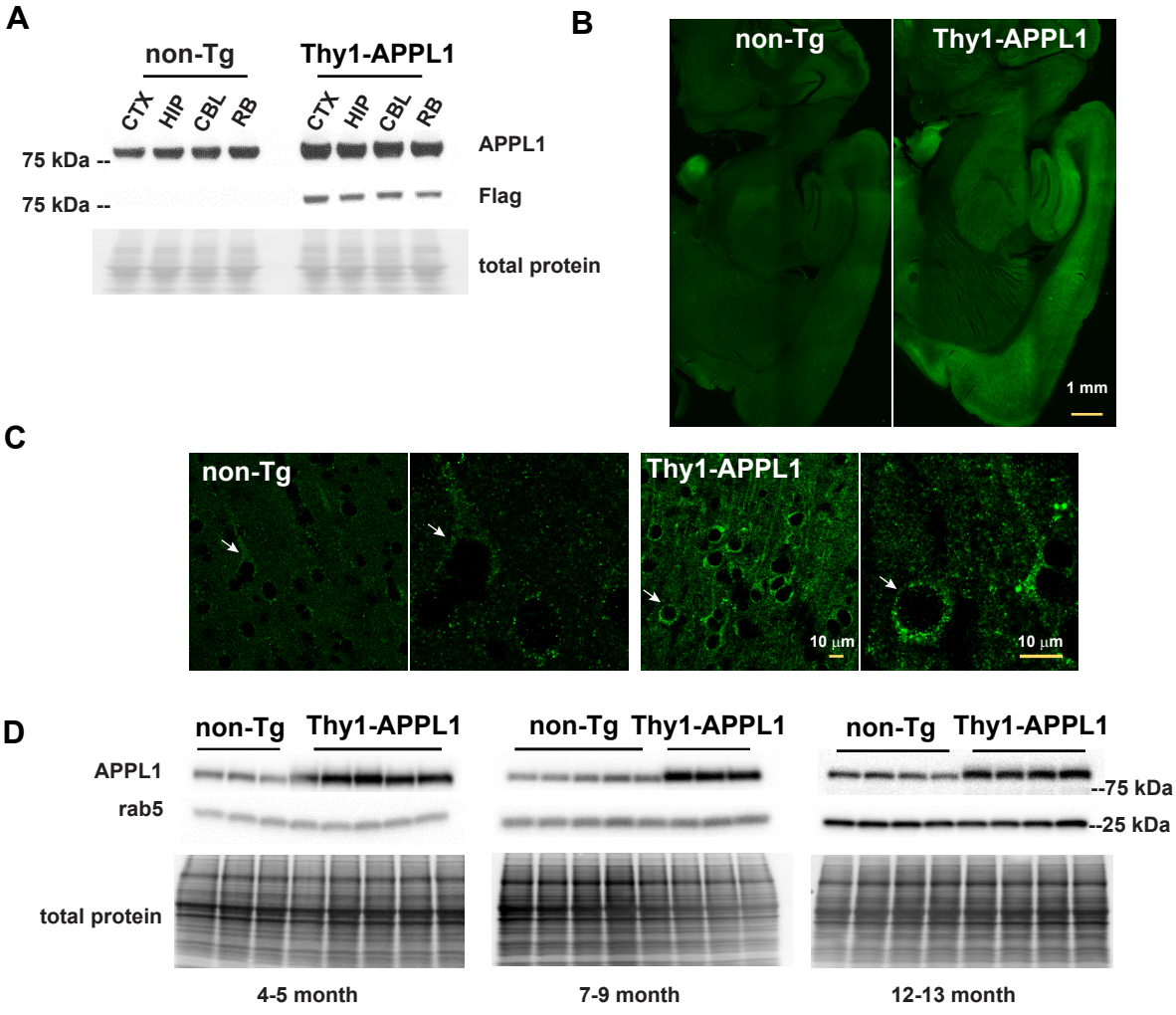
A
non-Tg
Thy1-APPL1
CTX
HIP
CBL
RB
CTX
HIP
CBL
RB
75 kDa --
75 kDa --
APPL1
Flag
total protein
B
non-Tg
Thy1-APPL1
1 mm
C
non-Tg
Thy1-APPL1
10 µm
10 µm
D
non-Tg
Thy1-APPL1
non-Tg
Thy1-APPL1
non-Tg
Thy1-APPL1
APPL1
rab5
--75 kDa
--25 kDa
total protein
4-5 month
7-9 month
12-13 month
E
Protein level rel. WT
0
1
2
3
4
**
***
***
non-Tg
Thy1-APPL1
APPL1
rab5
APPL1
rab5
APPL1
rab5
4-5 month
7-9 month
12-13 month

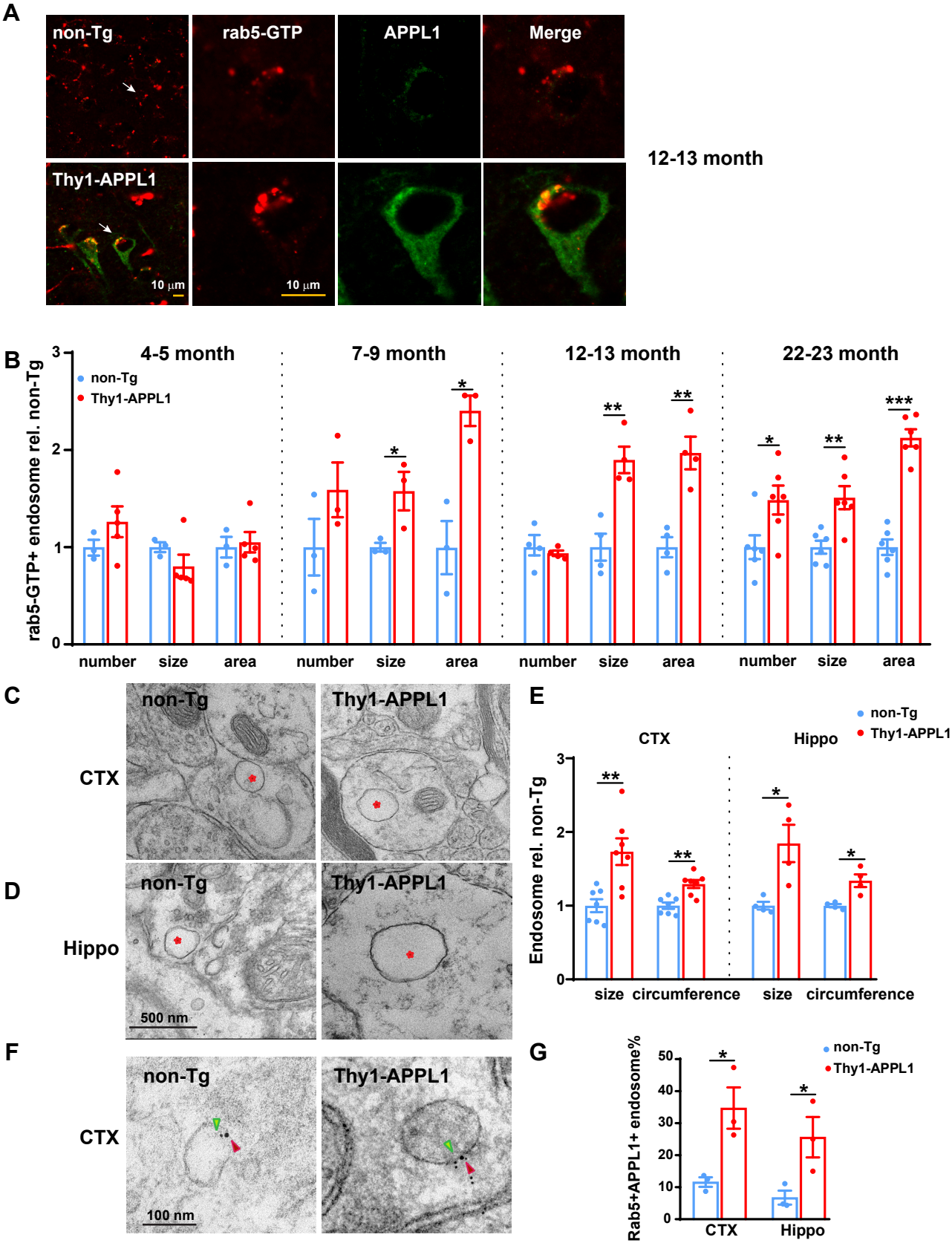
A
non-Tg
rab5-GTP
APPL1
Merge
Thy1-APPL1
10 μm
10 μm
12-13 month
B
4-5 month
7-9 month
12-13 month
22-23 month
non-Tg
Thy1-APPL1
rab5-GTP+ endosome rel. non-Tg
number
size
area
C
CTX
non-Tg
Thy1-APPL1
D
Hippo
500 nm
E
CTX
Hippo
Endosome rel. non-Tg
size
circumference
F
CTX
100 nm
G
Rab5+APPL1+ endosome%
CTX
Hippo

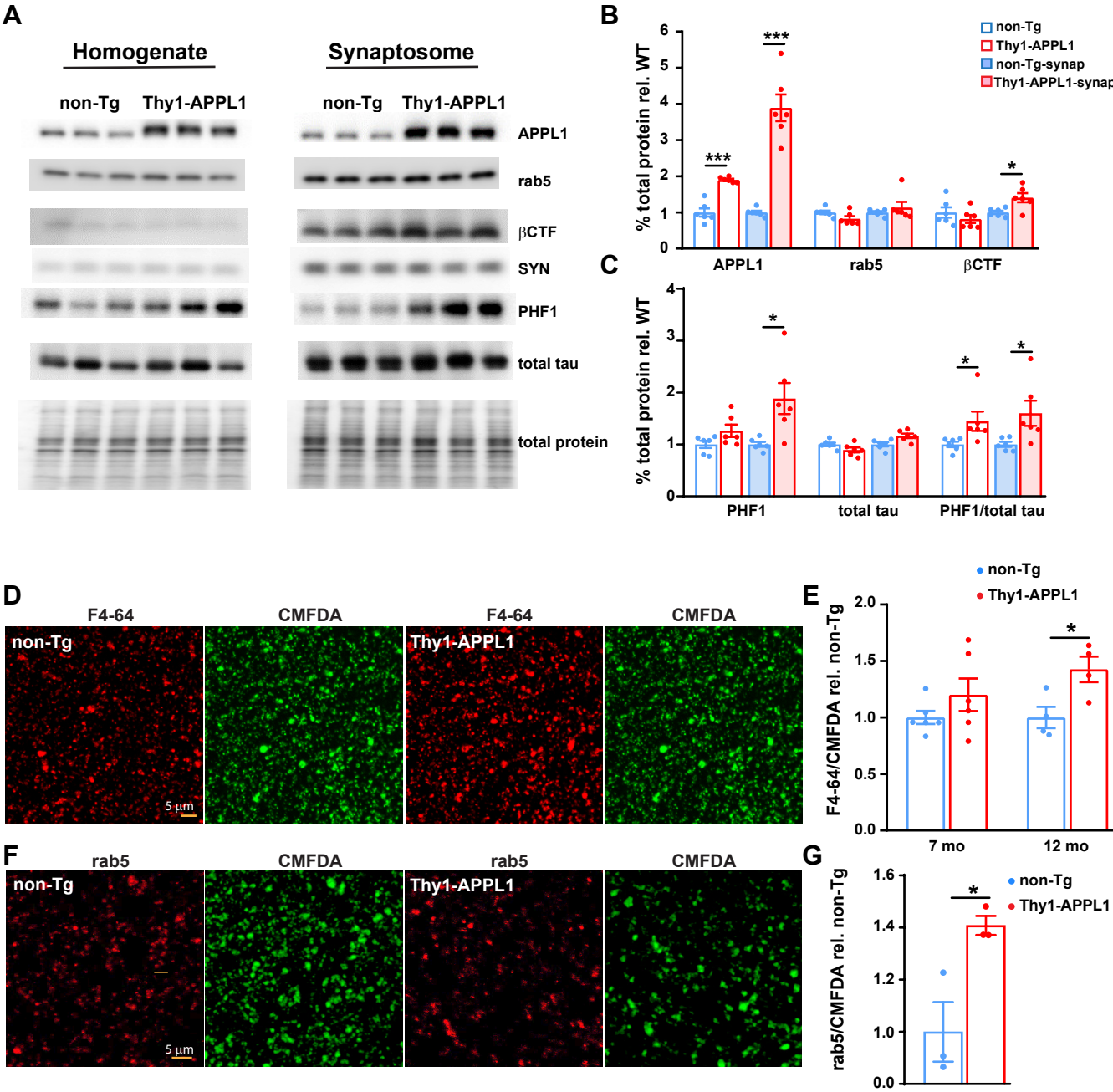
A
Homogenate
Synaptosome
non-Tg
Thy1-APPL1
non-Tg
Thy1-APPL1
APPL1
rab5
βCTF
SYN
PHF1
total tau
total protein
B
non-Tg
Thy1-APPL1
non-Tg-synap
Thy1-APPL1-synap
% total protein rel. WT
APPL1
rab5
βCTF
C
% total protein rel. WT
PHF1
total tau
PHF1/total tau
D
F4-64
CMFDA
F4-64
CMFDA
non-Tg
Thy1-APPL1
5 µm
E
non-Tg
Thy1-APPL1
F4-64/CMFDA rel. non-Tg
7 mo
12 mo
F
rab5
CMFDA
rab5
CMFDA
non-Tg
Thy1-APPL1
5 µm
G
non-Tg
Thy1-APPL1
rab5/CMFDA rel. non-Tg

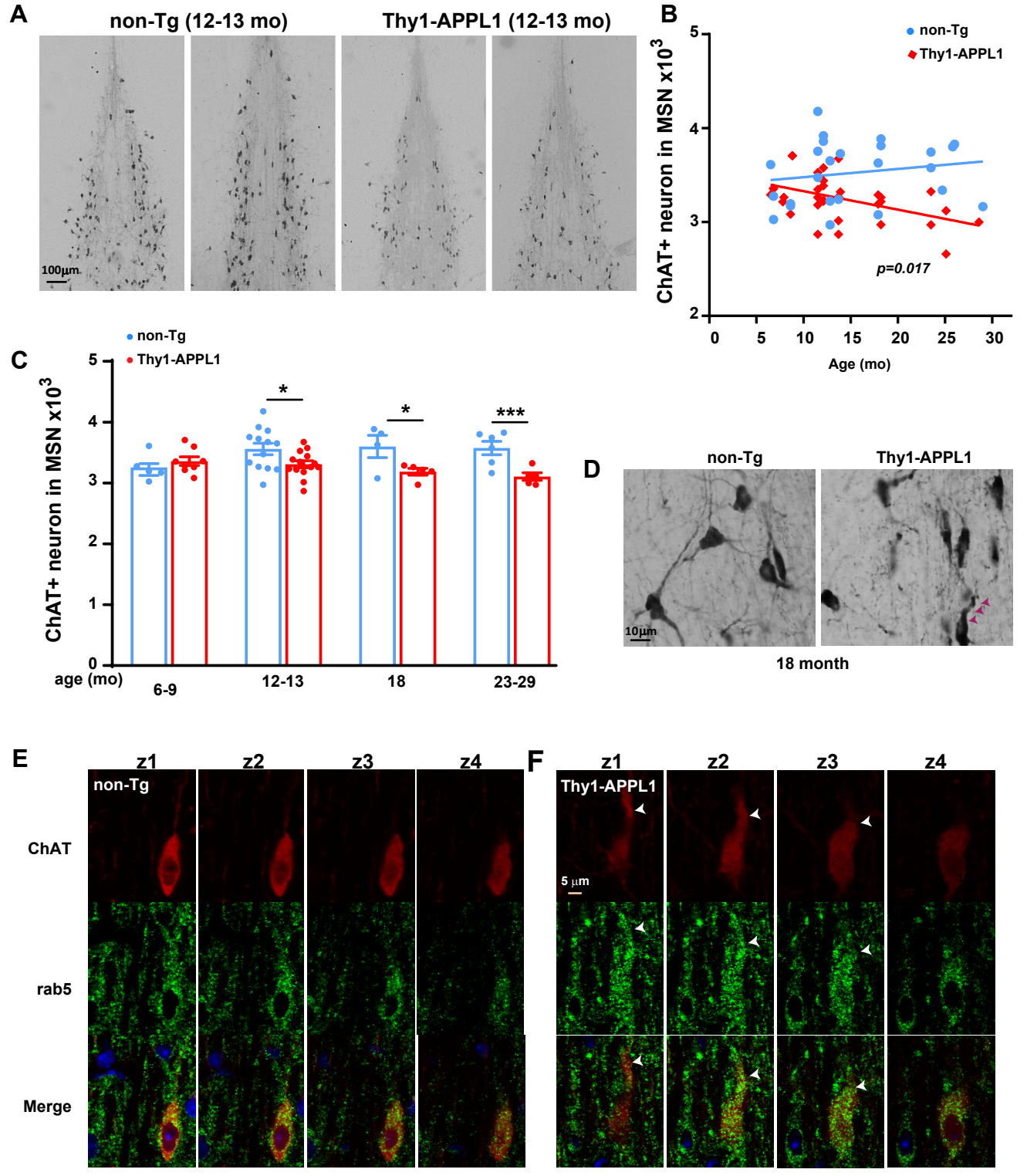
A
non-Tg (12-13 mo)
Thy1-APPL1 (12-13 mo)
100µm
B
non-Tg
Thy1-APPL1
ChAT+ neuron in MSN x10^3
p=0.017
Age (mo)
C
non-Tg
Thy1-APPL1
ChAT+ neuron in MSN x10^3
*
*
***
age (mo)
6-9
12-13
18
23-29
D
non-Tg
Thy1-APPL1
10µm
18 month
E
z1
z2
z3
z4
non-Tg
ChAT
rab5
Merge
F
z1
z2
z3
z4
Thy1-APPL1
5 µm

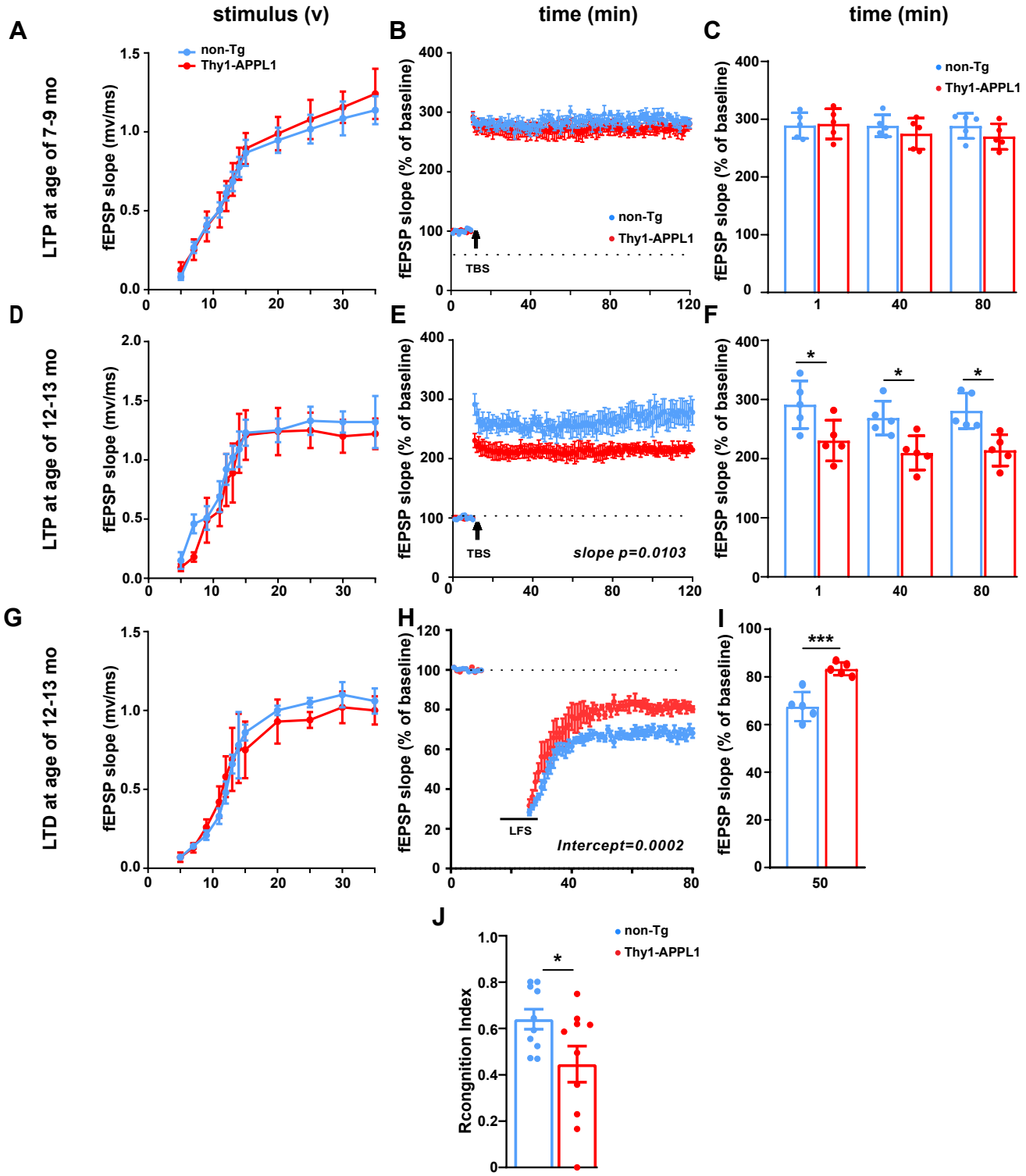
A
stimulus (v)
LTP at age of 7-9 mo
fEPSP slope (mv/ms)
non-Tg
Thy1-APPL1
B
time (min)
fEPSP slope (% of baseline)
TBS
C
time (min)
D
LTP at age of 12-13 mo
E
slope p=0.0103
F
G
LTD at age of 12-13 mo
H
LFS
Intercept=0.0002
I
J
Rcongnition Index